Improvements in Cloud Photogrammetry Using Airborne, Side-Looking, Time-Lapse Cameras

CLEON J. BITER, THEODORE W. CANNON[1], EDWIN L. CROW, CHARLES A. KNIGHT AND PHILIP M. ROSKOWSKI

National Center for Atmospheric Research[2], Boulder, CO 80307

(Manuscript received 27 May 1982, in final form 14 January 1983)

ABSTRACT

An airborne photographic system, in which the cameras are coupled with an inertial navigation system, was developed and used in a 1978 convective cloud study. Photogrammetric analysis from such a system is enhanced: cloud-feature positions can be determined without external references such as the earth's horizon or cloud base in the photographs, and the data reduction process can be considerably automated.

This paper describes the instrumentation, the photogrammetric theory, and the procedures for obtaining cloud measurements from the photographs. An empirical error analysis based on photographs of terrestrial targets is also presented. Cloud top heights determined without any reference height in the photographs are considered to be accurate to within 440 m at a range of 60 km. The largest source of error in determining cloud top height using the 1978 measurements is the uncertainty in determining the aircraft-to-cloud distance rather than inaccuracy in the photographic system. This error can be reduced in future programs by flying as closely in altitude as possible to the cloud features of interest.

1. Introduction

Airborne time-lapse cameras are not new in atmospheric science experiments (e.g., Whitney and McClain, 1967; Warner, 1978; Holle, 1982). They have been used in studies including the determination of size distributions of cumulus cloud populations (Plank, 1969; Warner, 1981), the measurement of convective cloud growth (Cantilo and Woodley, 1970), and the motions of cumulus clouds (Fujita *et al.*, 1975).

In 1978, the Convective Storms Division of the National Center for Atmospheric Research (NCAR) with assistance from the NCAR Research Aviation Facility developed an airborne photographic system for use in a convective field experiment in northeast Colorado. The airborne instrumentation and particularly the associated data analysis procedures differ sufficiently from other versions to warrant description. The advantages of the present system stem mainly from the use of an inertial navigation system (INS) to measure the position and the attitude of the aircraft (cameras) with respect to the earth at the exact time of exposure. These measurements allow cloud feature positions to be determined from photographs that do not contain external references such as the earth's horizon, cloud base or cloud anvil. In addition, the data reduction process can be automated considerably. Matrix algebra can be used and assumptions that have frequently been necessary in the past and limit data accuracy, such as constant aircraft ground speed and drift angle, are not required. While the underlying concepts for these improvements are not new in the general field of photogrammetry (see Slama, 1980), to the authors' knowledge they have not been exploited in cloud photogrammetry.

The following sections describe the relevant instrumentation, photogrammetric principles, equations, and data reduction procedures. An error analysis is also presented. Examples of photogrammetric measurements from the system are compared with radar measurements in growing cumuli in Knight *et al.* (1983).

2. Equipment

An NCAR Beechcraft Queen Air equipped with a recording system and meteorological instrumentation including a Litton LTN-51 inertial navigation system (INS) was used as the airborne photographic platform. The INS uses a triad of gyros and accelerometers to measure aircraft accelerations and attitude angles. These instruments are mounted on a gimbaled platform that is continually torqued to stay aligned with the local earth vertical. Aircraft velocity and position are derived through integration of the accelerometer outputs; the aircraft attitude angles,

[1] Present Affiliation: Solar Energy Research Institute, Golden, CO 80401.

[2] The National Center for Atmospheric Research is sponsored by the National Science Foundation.

with respect to the earth, are measured by synchros and resolvers mounted on the platform gimbals. Additional information on the INS can be found in Broxmeyer (1964) and Kelley (1973).

Two Flight Research Model IIIB, 16 mm, time-lapse cameras with 10 mm focal-length Switar lenses were installed "looking" out each side of the aircraft with the lenses pointed upward approximately 7°. Each camera was equipped with side fiducial marks and a data chamber that "printed" the time of exposure to the nearest 0.1 s along the edge of each frame of Kodachrome 25 film. The time of exposure, to the nearest 0.025 s, was also recorded on magnetic tape every 0.05 s along with data from the INS and meteorological sensors.

3. Photogrammetric principles

The location of a photographed object can be accurately determined provided the camera location and orientation, the camera and lens calibration constants, and the distance to the object are known. Since the primary purpose of the 1978 study was height measurement, the following discussion will have that emphasis; however, the principles apply equally well to measurements of lateral position.

a. Image formation

The basic geometry of a camera and the relation between the photographed object and the corresponding film image are depicted in Fig. 1. When an object is at an "infinite" distance from the camera, light rays from the object focus to form an image on the film plane, which is perpendicular to the optical axis and passes through the back focal point F'. The distance from the emergent nodal point to the focal point is called the focal length FL. For purposes of clarity in the following discussion, an imaginary positive-image plane is introduced. This plane is parallel to the film plane and intersects the front focal point F. Features in the positive-image plane are identical in size and shape to those on the developed film, assuming no distortion.

A camera coordinate system is now defined. It is a right-handed, orthogonal, Cartesian system with the origin at the incident nodal point. The X axis coincides with the optical axis and is positive toward the object being photographed, the Z axis is positive downward through the bottom of the camera, and the Y axis is perpendicular to the X-Z plane and is positive out the right side of the camera. This is not the normal photogrammetric system but has been chosen here because it is similar to the standard aeronautical coordinate system used extensively throughout this paper. A point P in the positive-image plane can be defined in the camera coordinate system where X_C equals the focal length and Y_C and Z_C are equal in magnitude to coordinate measurements of the corresponding point P' on the film. These components define an image position vector originating at the incident nodal point and terminating at point P in the imaginary positive-image plane.

Features in the positive-image plane are scaled-down versions of the photographed object. The amount of scaling is inversely proportional to the ratio of the magnitude of a vector to a point on the object that is imaged (object position vector in Fig. 1) to the magnitude of the image position vector. The scale factor SF can be expressed as

$$\mathrm{SF} = \frac{(X_O^2 + Y_O^2 + Z_O^2)^{1/2}}{(X_C^2 + Y_C^2 + Z_C^2)^{1/2}}, \qquad (1)$$

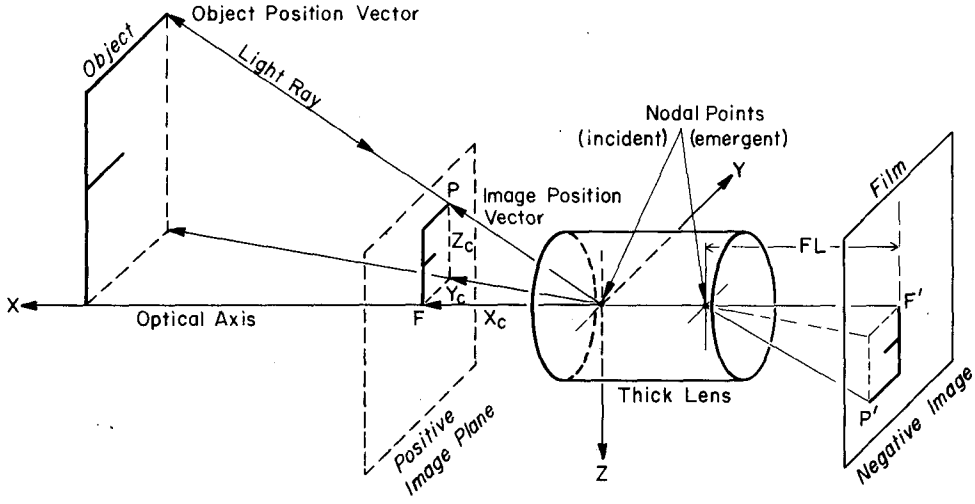

FIG. 1. Basic camera geometry and the relationship between a photographed object and the film image. (Adapted from Renick and Douglas, 1970).

where X_O, Y_O and Z_O are the coordinates of the object point in the camera coordinate system.

b. Height determination

Assume that the camera in Fig. 1 is oriented parallel to the ground; that is, the X-Y plane is level. If the horizontal distance D to the object is known, the height of the object or feature above the camera, or aircraft, is given by

$$Z_F = D \tan\theta, \tag{2}$$

where

$$\tan\theta = \frac{Z_C}{(X_C^2 + Y_C^2)^{1/2}} = \frac{Z_C}{(FL^2 + Y_C^2)^{1/2}}. \tag{3}$$

If D is unknown, it can be calculated from photographs taken from two different locations by means of Eq. (4), which is derived in the Appendix:

$$D\,(\text{km}) = 111.15\{(L_A - L_C)^2 + [(\lambda_A - \lambda_C)\cos L_A]^2\}^{1/2}, \tag{4}$$

where

$$\left.\begin{aligned} L_A &= \text{aircraft latitude}, & L_C &= \text{cloud latitude} \\ \lambda_A &= \text{aircraft longitude}, & \lambda_C &= \text{cloud longitude} \end{aligned}\right\}.$$

A means of correcting for the error in calculated distance due to cloud motion is also presented in the Appendix. This error can be significant, particularly if the cloud motion vector is parallel to the aircraft track.

Finally, the object height with respect to the earth can be calculated by accounting for the camera (aircraft) height and the effects of the earth's curvature and atmospheric refraction. According to Wolf (1974), the corrections to object height for atmospheric refraction R in the standard atmosphere and for the earth's curvature C may be combined and expressed as

$$(R + C) = 6.75 \times 10^{-5} D^2, \tag{5}$$

where $(R + C)$ and D are in kilometers.

If the aircraft or camera height is Z_A, then the height Z of the object with respect to the earth, assuming a level camera, is

$$Z = Z_F + (R + C) + Z_A. \tag{6}$$

c. Coordinate systems and transformations

Eq. (6) assumes a level camera, which is rarely the case in aerial photography. This section describes the coordinate systems and equations necessary to transform the film image coordinates from an airborne camera that is arbitrarily positioned and rotated in space to meaningful object coordinates with respect to the earth.

Fig. 2 shows the relevant right-handed, orthogonal, Cartesian coordinate systems. The aircraft system, denoted by the subscript A, utilizes standard aero-

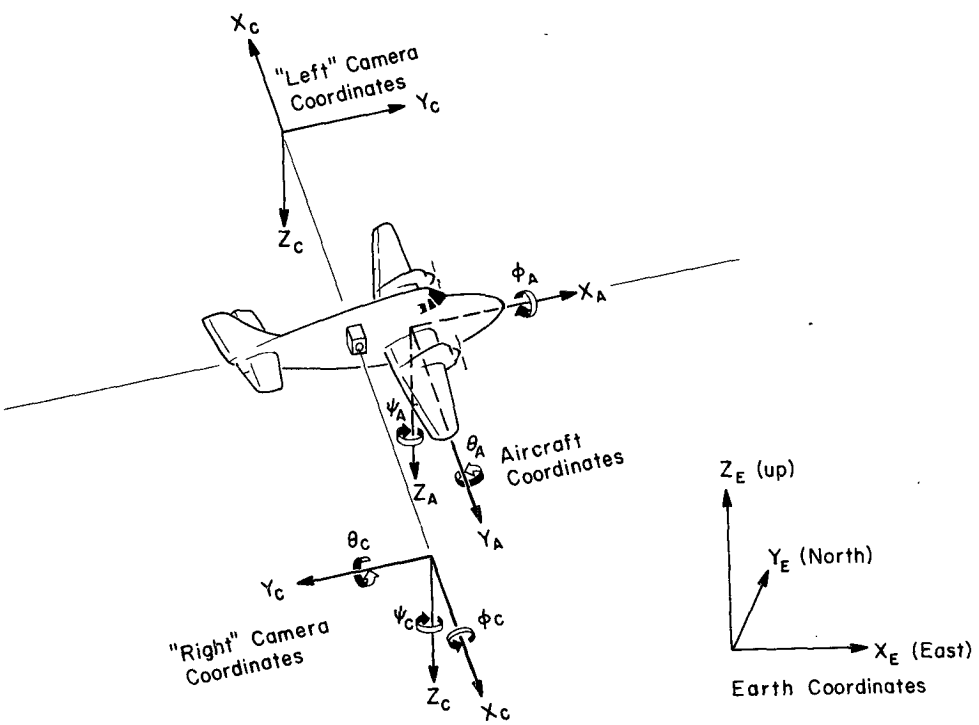

FIG. 2. The coordinate systems used in this study.

nautical conventions (e.g., Etkin, 1959). The origin is located at the aircraft center of gravity with the X axis in the aircraft plane of symmetry; its positive direction is forward along the aircraft longitudinal axis. The Y axis is perpendicular to the plane of symmetry and is positive out the right wing while the Z axis is perpendicular to the X-Y plane and is positive downward. It appears from Fig. 2 that two different camera coordinate systems are involved but they are identical with respect to each camera (see Section 3a); the apparent discrepancy arises because the cameras "look" out opposite sides of the aircraft. Both cameras, and hence the origins of their coordinate systems, can be (and are) assumed to be located at the aircraft center of gravity. A commonly used meteorological coordinate system has been chosen for use as the earth system; however, in this application its origin is also located at the aircraft center of gravity. The positive Z axis is directed upward parallel to the gravity vector, the X-Y plane is perpendicular to the Z axis with the X axis positive toward the east, and the Y axis positive toward true north.

Positive rotation angles for the aircraft and camera systems are also depicted in Fig. 2. Positive pitch θ is a rotation around the appropriate Y axis so that aircraft nose (or camera lens) rotates upward. Positive roll ϕ is a rotation around the X axis so that the right aircraft wing (or camera side) is lowered. Positive yaw ψ is a rotation around the Z axis in a clockwise manner as viewed from above. Thus, if the "right" camera is mounted perpendicular to the aircraft longitudinal axis, an aircraft roll of 10° appears to be a camera pitch of −10°.

The INS system on the NCAR Queen Air is stabilized along the local earth axes so that the rotation angles of the platform gimbals are equivalent to the aircraft attitude angles: aircraft pitch θ_A and roll ϕ_A are relative to the earth's horizontal plane and yaw (heading) ψ_A is relative to true north (Kelley, 1973). Camera attitude angles are defined with respect to the aircraft coordinate axes. If, for example, both side-looking cameras were orientated exactly perpendicular to the aircraft longitudinal axis and were tilted upwards 10°, then $\theta_C = 10°$, $\phi_C = 0°$ and $\psi_C = 90°$ for the right-side camera and $\theta_C = 10°$, $\phi_C = 0°$ and $\psi_C = 270°$ for the left-side camera. Since the cameras are rigidly fixed to the airframe, their attitude angles remain constant until the camera positions are purposely changed. These angles are determined through calibration.

Using the coordinate systems described above, the coordinates of the image position vector in the camera system (X_C, Y_C, Z_C) can be transformed into coordinates in the aircraft system (X_A, Y_A, Z_A), and then into coordinates in the earth system (X_E, Y_E, Z_E). In matrix notation, this transformation is given by

$$\begin{bmatrix} X_E \\ Y_E \\ Z_E \end{bmatrix} = [C_E^A][C_A^C] \begin{bmatrix} X_C \\ Y_C \\ Z_C \end{bmatrix}, \tag{7}$$

where $[C_E^A]$ and $[C_A^C]$ are, respectively, the 3 × 3 rotation matrices for the aircraft to earth, and camera to aircraft system transformations. For the general case of the arbitrarily oriented camera the earth-referenced image position coordinates from Eq. (7) are substituted in place of X_C, Y_C and Z_C in Eq. (3).

Both of the rotation matrices have the general form of a positive rotation from system 1 to 2 as expressed in Eq. (8):

$$[C_2^1] = \begin{bmatrix} \cos\psi' \cos\theta' & \cos\psi' \sin\theta' \sin\phi' + \sin\psi' \cos\phi' & -\cos\psi' \sin\theta' \cos\phi' + \sin\psi' \sin\phi' \\ -\sin\psi' \cos\theta' & -\sin\psi' \sin\theta' \sin\phi' + \cos\psi' \cos\phi' & \sin\psi' \sin\theta' \cos\phi' + \cos\psi' \sin\phi' \\ \sin\theta' & -\cos\theta' \sin\phi' & \cos\theta' \cos\phi' \end{bmatrix}. \tag{8}$$

In the present application, the rotation angles are modified in accordance with the following:

For camera to aircraft coordinates

$$\left.\begin{aligned} \phi' &= -\phi_C \\ \theta' &= -\theta_C \\ \psi' &= -\psi_C \end{aligned}\right\}. \tag{9}$$

For aircraft to earth coordinates

$$\left.\begin{aligned} \phi' &= -(\phi_A - 180°) && Z \text{ is now positive upward} \\ \theta' &= \theta_A && X \text{ is now positive toward east} \\ \psi' &= (\psi_A - 90°) && Y \text{ is now positive toward north} \end{aligned}\right\}. \tag{10}$$

4. Data reduction

Images on a 16 mm film are too small to enable accurate measurements to be made directly on the film; hence, the film is projected to enlarge the features to a convenient size (a magnification of 60 was used in this study). Ultimately, the features are referenced to an orthogonal X, Y coordinate system il-

lustrated in Fig. 3. The origin is located at the principal point—the intersection of the optical axis with the film plane—and the X axis parallels a line connecting the fiducial marks. However, to reduce the potential for errors, no measurements are actually made during the projection process. The analyst simply marks the projected locations of the fiducial marks and the features of interest on paper, and records the time the frame was exposed from the data block. The coordinates of features with respect to the fiducials are measured later.

These coordinates, the time of exposure, and the aircraft-to-cloud distance or the times of two photographs to be used for triangulation plus cloud motion are input into the computer program. There, the fiducial coordinates are translated into coordinates X_p and Y_p relative to the principal point and then into camera coordinates using the following expressions, where M_p is the magnification of the projected image:

$$X_C = \text{FL}, \tag{11}$$

$$Y_C = X_P(1/M_p), \tag{12}$$

$$Z_C = -Y_P(1/M_p). \tag{13}$$

Using Eq. (7) and the aircraft altitude and attitude angles from tape at the exact time (±0.025 s) of exposure, the camera coordinates are transformed into earth coordinates, scaled to size with Eq. (1), adjusted for aircraft altitude, and corrected for refraction and earth's curvature to yield the desired cloud feature height.

Provisions in the program also enable the analyst to enter corrections to the aircraft position data that have been recorded from the INS. These data contain errors that "drift" with time and should be corrected if "updates" are available. INS position errors, as a function of time since alignment, are discussed by Lenschow (1972) for a system similar to that on the Queen Air.

5. Calibrations and error analysis

Eq. (14) is Eq. (6) with appropriate substitutions:

$$Z = D\tan\theta + 6.75 \times 10^{-5}D^2 + Z_A, \tag{14}$$

where

- Z height of the photographed object above the earth
- D distance between the camera and the object
- θ elevation angle of the object above the camera
- Z_A aircraft (camera) height above the earth.

It can be seen that errors in object height calculations can come from three sources: photographic system errors (errors in θ), positioning errors of either the aircraft or cloud (errors in D and Z_A), and differences between refraction in the actual and the standard atmosphere that is assumed. These error sources are now discussed; the resulting errors will be expressed as angles applicable at the principal point (the center of the film), which is the worst case.

a. Photographic system errors

The system accuracy can be estimated from the calibration data for the camera attitude angles. By virtue of the manner in which the calibrations were

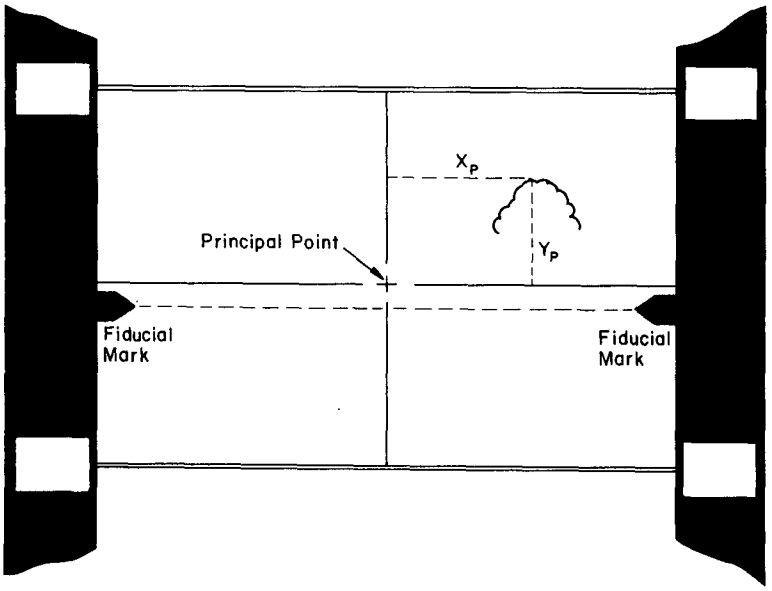

FIG. 3. The film frame coordinate system. The origin is located at the principal point and the X axis is parallel to a line connecting the fiducial images.

performed, the data inherently contain the effects of all sources of errors including calibrations, projection, measurement and computations. During each research flight, two calibration "legs" were flown above a prescribed ground track several kilometers long while calibration targets at known locations on either side of the aircraft were photographed at a rate of one frame per second. The camera attitude angles were then computed from measurements made in each frame of the projected processed films.

Since the cameras had been mounted almost perpendicular (<1° difference) to the aircraft longitudinal axis, the camera roll angles ϕ_C were determined by measuring the apparent "tilt" of the earth's horizon with respect to the fiducials and correcting the "tilt" by the amount of aircraft pitch. The two remaining attitude angles, camera pitch θ_C and camera yaw ψ_C were determined by solving Eq. (7) iteratively for the unique combination of angles that would produce the measured film coordinates given the location and attitude of the aircraft and the earth coordinates of the photographed object. Earth-referenced components of the image position vector were scaled to size with Eq. (1) during these computations.

Values of the camera pitch and yaw angles determined by this technique contain leg-to-leg and flight-to-flight variance introduced by "small" inaccuracies in aircraft positioning. Since the calibration targets were 3220 m from either side of the aircraft, an error of only 5.6 m in positioning the aircraft in a fore–aft direction along its longitudinal axis is equivalent to an error of 0.1° in the calculated camera yaw. Similarly, an error of 5.6 m in aircraft altitude is equivalent to an error of 0.1° in the calculated camera pitch. The required aircraft position accuracy exceeds even the resolution of the recorded position. An initial position for the aircraft at the beginning of each leg was determined using aircraft-measured static pressure and a triangulation process involving photographs from both sides of the aircraft; the subsequent positions along a leg were computed by adding integrated INS accelerations to the initial position. As a consequence, the calculated mean values of the attitude angles for any given calibration leg can be expected to be biased as a result of errors in the calculated initial position. In order to remove the leg-to-leg and flight-to-flight variance due to these positioning errors, the calibration data have been analyzed with a two-way nested classification variance component model with unbalanced data given by Searle (1971).

Table 1 contains the results of this analysis applied to the calibration data for eight flights spanning the 1978 research period. The overall accuracy of the system is proportional to our ability to determine the true mean value of the camera attitude angles. In the case of camera pitch, which is the most important angle in height determination, we are 95% confident

TABLE 1. Results from the analysis of variance of the camera attitude angle calibration data. All entries in degrees.

	Port camera angles			Starboard camera angles		
	θ_C	ϕ_C	ψ_C	θ_C	ϕ_C	ψ_C
Mean	7.64	0.23	−0.62	6.36	0.56	1.63
Standard deviation of the mean	0.06	0.09	0.13	0.13	0.06	0.16
	Standard deviation of the components					
Flight-to-flight	0.11	0.24	0.00	0.34	0.16	0.22
Leg-to-leg	0.15	0.00	0.52	0.19	0.00	0.54
Frame-to-frame	0.13	0.22	0.15	0.13	0.22	0.20
	Summary statistics for camera pitch θ_C					
Accuracy	0.11			0.26		
Precision	0.25			0.26		

that the calibration values for the port and starboard cameras are, respectively, within 0.11° and 0.26° of their true values. The precision of the system is proportional to how closely we can make repeated measurements of the same object from frame to frame. This precision, estimated here as twice the standard deviation of the frame-to-frame measurements, is 0.25° for the port camera and 0.26° for the starboard camera. This frame-to-frame variation can be reduced by smoothing over a sequence of frames. Variations in the data from flight to flight and leg to leg have been disregarded in deriving the precision estimate because they result from the positioning inaccuracies that affect the calibration data but are not applicable to cloud height computations.

During the analysis of the high-contrast calibration data, the target positions could be measured to 0.5 mm (at a magnification of 60), which is equivalent to 0.05°. Cloud features photographed during research typically provided less contrast and could only be measured to 1 mm (0.1°). Smoothing over a number of frames also compensates for this poorer resolution.

b. Positioning errors

Cloud height errors are also caused by errors in aircraft altitude Z_A or in the computation of the aircraft-to-cloud distance D. Aircraft altitude errors cause identical errors in cloud height calculations; however, the errors are small (<10 m) and have been neglected.

Errors in calculated distance can result from positioning errors of either the cloud or the aircraft or from unaccounted-for cloud motion (e.g., see Appendix). When Eq. (14) is differentiated with respect to distance, the only term of consequence is $dD \tan\theta$.

In the present study, the angular elevation θ was usually near 10°; the aircraft-to-cloud distance error is estimated to be less than or equal to 2 km since aircraft position "updates" and cloud motion compensation were utilized. Thus, any height errors due to distance errors are less than or equal to 350 m.

It is important to note that height errors due to positioning errors can be reduced by decreasing the vertical angle θ; therefore, the photography aircraft should be flown as closely as possible in altitude to the feature of interest.

c. Refraction errors

The final error affecting cloud height accuracy results from differences in optical refraction in the actual versus the assumed standard atmosphere. According to Schut (1969), the difference in refraction in the standard atmosphere which has been assumed here and the supplemental tropospheric atmosphere for the summer (July) is less than 8 μrad at the altitudes of interest. This difference results in an error of less than 1 m at the largest aircraft-to-cloud distances in this study; therefore, height errors due to errors in the assumed refractive index are neglected.

d. Combined effects of errors

Table 2 summarizes the effects of the two main sources of errors on cloud height calculations for the range of aircraft to cloud distances used during the 1978 experiment. The upper error bound combines the uncertainty in the true mean camera pitch angle and the uncertainty in estimating the distance to the cloud. It is assumed in the table that the pitch angle variation from frame to frame has been smoothed out by applying a running filter over a sequence of frames. At the normal distances of 40–60 km used in the 1978 study, the potential error in calculated cloud heights is less than 440 m. Error values are also given for the extreme distances of 25 and 110 km that were used once.

Notice that the main source of error is not due to errors in the photographic system but due to the distance error, which, in turn, is a function of the angle that the photographed object is above or below the aircraft. It is evident that the estimated contribution of 350 m is quite a rough upper bound, arising from the distance error bound of 2 km and the elevation angle of 10°. Again, this error can be reduced by flying, as nearly as possible, at the same altitude as the cloud feature of interest.

TABLE 2. Error bound (m) in calculated cloud feature heights as a function of aircraft-to-cloud distance and individual error sources assuming frame-to-frame variations have been smoothed out.

	Aircraft-to-cloud distance (km)			
Error sources	25	40	60	110
Uncertainty in mean camera pitch angle (starboard camera, 0.26°)	110	180	270	450
Distance error (2 km, θ = 10°)	350	350	350	350
Root sum square	370	390	440	570

6. Conclusions

An airborne, side-looking, time-lapse photographic system was developed in which the photographic data are coupled with aircraft position and attitude data from an onboard inertial navigation system. The resulting data reduction process is largely automated and cloud feature positions can be determined from photographs that do not contain external reference features such as cloud base or the earth's horizon.

An error analysis of the system, based on photographs of terrestrial calibration targets, indicates that errors in calculated cloud heights are less than 440 m for the distances normally used in this study. These errors come from two main sources: photographic system errors and incorrect calculations of the aircraft-to-cloud distance. The predominate error source, due to distance errors, can be easily minimized in future experiments by flying as closely as possible to the altitude of the feature of interest.

Acknowledgments. The authors thank Ron Holle and Richard Decker of the National Oceanographic and Atmospheric Administration for helpful discussions and advice during the initial stages of this work. We also thank the personnel of the NCAR Research Aviation Facility, particularly Norman Zrubek and Charles Cullian, for assistance in instrumenting the aircraft, and Lester Zinser for his enthusiastic role as pilot. We especially thank Daniel Breed of the Convective Storms Division for operating the cameras on several of the research flights and for critically reviewing this paper. We express our gratitude to Carol Brown, Sharon Blackmon and Susan Thomas for typing the manuscript.

APPENDIX

Triangulation

This appendix presents the derivation of the equation to calculate the horizontal distance between the aircraft and cloud feature using photographs of the cloud taken from two different locations. The equation is first derived for the special case in which the cloud is stationary and is then modified to account for cloud motion.

Fig. A1 shows the geometry relevant to the problem. The known parameters consist of the latitude L_A and longitude λ_A of the aircraft at positions 1 and

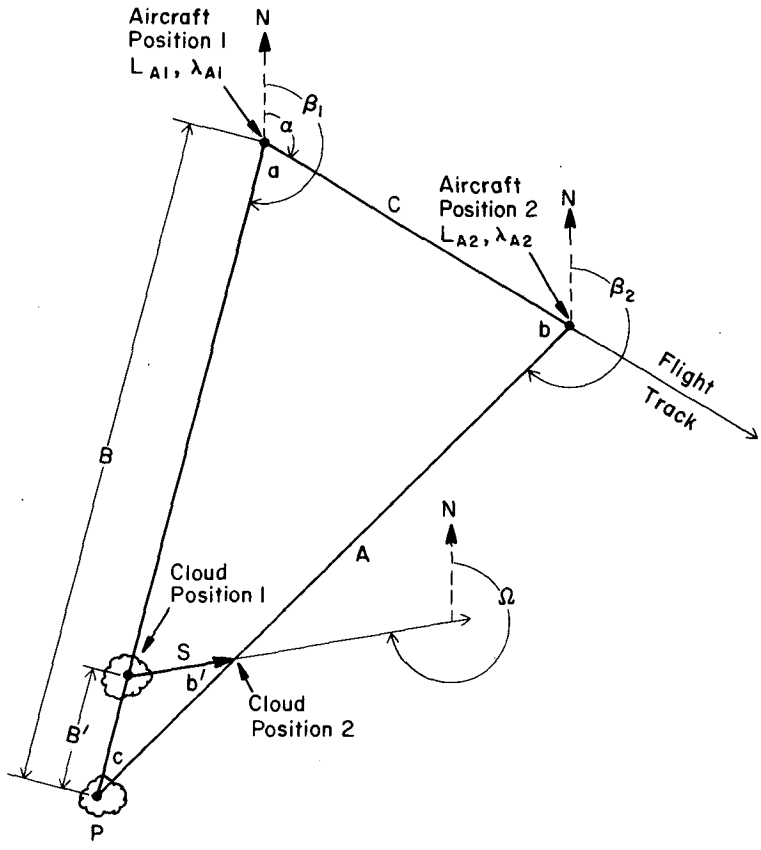

FIG. A1. Geometry relevant to the calculation of aircraft-to-cloud distance. The distance is computed on the basis of cloud pictures taken from the aircraft at positions 1 and 2.

2 and the X and Y film coordinates that have been rotated into the earth coordinate system. The derivation of these earth-referenced coordinates X_E and Y_E is presented in Section 3c.

First, assume a stationary cloud at position P. From the law of sines

$$B = \frac{C \sin b}{\sin c} = \frac{C \sin|\beta_2 - \alpha|}{\sin|\beta_2 - \beta_1|}, \tag{A1}$$

where

$$\beta_1 = \tan^{-1}\frac{X_E}{Y_E} \quad \text{at position 1,} \tag{A2}$$

$$\beta_2 = \tan^{-1}\frac{X_E}{Y_E} \quad \text{at position 2.} \tag{A3}$$

The distance C and heading α between aircraft positions 1 and 2 are calculated using standard great-circle navigation equations:

$$C\,(\text{nm}) = 60 \cos^{-1}[\sin L_{A1} \sin L_{A2} + \cos L_{A1} \cos L_{A2} \cos(\lambda_{A2} - \lambda_{A1})], \tag{A4}$$

$$\alpha = \cos^{-1}\left[\frac{\sin L_{A2} - \sin L_{A1} \cos\left(\frac{C}{60}\right)}{\sin\left(\frac{C}{60}\right) \cos L_{A1}}\right]. \tag{A5}$$

If $\sin(\lambda_{A1} - \lambda_{A2}) < 0$, then $\alpha = 360° - \alpha$.

The latitude and longitude of the cloud (L_C and λ_C) can now be calculated by

$$L_C = L_{A1} + \frac{B \cos\beta_1}{60}, \tag{A6}$$

$$\lambda_C = \lambda_{A1} - \frac{B \sin\beta_1}{60 \cos L_{A1}}, \tag{A7}$$

and finally the horizontal distance D from aircraft to cloud at any time is expressed by

$$D\,(\text{km}) = \frac{6076}{3280}\{[(L_A - L_C)60]^2 + [(\lambda_A - \lambda_C)60 \cos L_A]^2\}^{1/2}. \tag{A8}$$

We now assume that the cloud has a velocity such

that it moves from cloud position 1 to cloud position 2 during the time the aircraft has flown from position 1 to position 2. This velocity is defined using the normal meteorological wind convention in which the speed S is in knots and the direction Ω is the direction, with respect to true north, from which the cloud moves. If we incorrectly assume the cloud is stationary we will calculate its distance from the aircraft at time t_1 as equal to B which is in error by B'.

The correct distance from aircraft to cloud is $B - B'$ where B is calculated by Eq. (A1) and B' is calculated by Eq. (A9), i.e.,

$$B' = \frac{S \sin|\beta_2 - \Omega|}{\sin|\beta_2 - \beta_1|}. \quad \text{(A9)}$$

The latitude L_{C1} and longitude λ_{C1} of the cloud at time t_1 are calculated by substituting $(B - B')$ in place of B in (A6) and (A7) and the cloud position at any time t_N after t_1 is now obtained by computing the cloud movement during the time interval $t_N - t_1$, and adding this displacement to the initial position. That is,

$$L_{CN} = L_{C1} + \Delta L_C$$
$$= L_{C1} - S(\cos\Omega)(2.16 \times 10^{-5})(t_N - t_1), \quad \text{(A10)}$$
$$\lambda_{CN} = \lambda_{C1} + \Delta\lambda_C$$
$$= \lambda_{C1} - S(\sin\Omega)\left(\frac{2.16 \times 10^{-5}}{\cos L_{CN}}\right)(t_N - t_1), \quad \text{(A11)}$$

where $(t_N - t_1)$ is expressed in seconds.

The correct aircraft-to-cloud distance D at any time t_N for this case where the cloud moves is still calculated by Eq. (A8) by substituting L_{CN} and λ_{CN} for L_C and λ_C, respectively.

A different procedure to compensate for cloud motion is presented by Warner (1981).

REFERENCES

Broxmeyer, C., 1964: *Inertial Navigation Systems.* McGraw-Hill, 254 pp.

Cantilo, L. M. H., and W. L. Woodley, 1970: Cloud photogrammetry from airborne time-lapse photography. *J. SMPTE,* **79,** 604–606.

Etkin, B., 1959: *Dynamics of Flight.* Wiley, 519 pp.

Fujita, T. T., E. W. Pearl and W. E. Shenk, 1975: Satellite-tracked cumulus velocities. *J. Appl. Meteor.,* **14,** 407–413.

Holle, R. L., 1982: Photogrammetry of thunderstorms. *Thunderstorms: A Social, Scientific and Technological Documentary,* Vol. 3. Government Printing Office, 77–98.

Kelley, N. D., 1973: Meteorological uses of inertial navigation. *Atmospheric Technology,* No. 1, NCAR, 37–39 (Unpublished ms.).

Knight, C. A., W. D. Hall and P. M. Roskowski, 1983: Visual cloud histories related to first radar echo formation in northeast Colorado cumulus. *J. Appl. Meteor.,* **22,** 1022–1040.

Lenschow, D. H., 1972: The measurement of air velocity and temperature using the NCAR Buffalo aircraft measuring system. NCAR Tech. Note NCAR-TN/EDD-74, 39 pp.

Plank, V. G., 1969: The size distribution of cumulus clouds in representative Florida populations. *J. Appl. Meteor.,* **8,** 46–67.

Renick, J. H., and R. H. Douglas, 1970: Cloud photogrammetry. Stormy Weather Group, Tech. Rep. MWT-7, McGill University, 11 p.

Schut, 1969: Photogrammetric refraction. *Photogramm. Eng.,* **35,** 79–87.

Searle, S. R., 1971: *Linear Models.* Wiley, 532 pp.

Slama, C. C., Ed., 1980: *Manual of Photogrammetry.* Amer. Soc. Photogramm., Falls Church, VA, 1056 pp.

Warner, C., 1978: Photogrammetry from aircraft nose camera movies. *J. Appl. Meteor.,* **17,** 1416–1420.

——, 1981: Photogrammetry from aircraft side camera movies: Winter MONEX. *J. Appl. Meteor.,* **20,** 1516–1526.

Whitney, L. F., Jr., and E. P. McClain, 1967: Cloud measurements using aircraft time-lapse photography. Tech. Rep. ESSA-40, Washington, DC, 24 pp.

Wolf, P. R., 1974: *Elements of Photogrammetry.* McGraw-Hill, 562 pp.